# 8.4 EVALUATION OF THE IMPACTS OF INGESTING TRMM DATA ON THE ACCURACY OF QUANTITATIVE PRECIPITATION ESTIMATES OBTAINED VIA THE SCaMPR FRAMEWORK

Yu Zhang[1*], Robert Kuligowski[2], David Kitzmiller[1], Dong-Jun Seo[1,3], and Yaping Li[2,4]

[1]Office of Hydrologic Development, NOAA National Weather Service, Silver Spring MD
[2]Center for Satellite Applications and Research, NOAA National Environmental Satellite, Data, & Information Service, Camp Spring, Maryland
[3]University Corporation for Atmospheric Research, Boulder, Colorado…..
[4]I. M. Systems Group, Lanham, Maryland

## 1. INTRODUCTION

The Tropical Rainfall Measurement Mission (TRMM) satellite, since its launch in 1997, has been proven an invaluable source of precipitation information over the tropics where large areas are not covered by ground sensors. One potential beneficiary of the TRMM-based quantitative precipitation estimates (QPE) is the National Weather Service (NWS) hydrologic forecasting operation which covers areas where precipitation data from ground-based sensors are often scarce to nonexistent. However, the infrequent temporal sampling of the TRMM data has been an obstacle to its direct utilization in such operations where frequent updates of precipitation data are required. One way to address this limitation is to combine TRMM QPE with more frequent measurements from Geostationary Operational Environmental Satellites (GOES). The Self-Calibrating Multivariate Precipitation Retrieval (SCaMPR) framework (Kuligowski 2002), developed at the NOAA's National Environmental Satellite, Data, and Information Service (NESDIS), serves this purpose. The original version of SCaMPR uses less frequent, but more accurate passive microwave (PM) precipitation estimates from the Defense Meteorological Satellite Program (DMSP) to calibrate the GOES infrared (IR) brightness temperature-to-rain rate relationship in real-time. This framework has been modified to allow ingesting TRMM data as an additional source of calibration data. In comparison to other existing multi-satellite QPE algorithms, such as the National Centers for Environmental Predictions (NCEP) Climate Prediction Center (CPC) Morphing (CMORPH; Joyce et al., 2004), and the TRMM Multi-satellite Precipitation Analysis (TMPA; Huffman et al. 2007), SCaMPR has the advantage of shorter latency, which is critical to NWS hydrologic predictions.

Prior to the experimental use of SCaMPR data in NWS hydrologic forecasting, NESDIS and NWS conducted a set of evaluation experiments to assess the potential improvement in the accuracy of QPE resulting from the ingest of TRMM data. The study site of the experiment was set to be central Texas which is within the effective latitude range of TRMM (i.e., below 35 degree latitude). The analyses were performed at hourly and daily resolutions by using a set of rain gauge measurements from the Lower Colorado River Authority (LCRA) for the period of 2000-7.

## 2. DATA AND METHODOLOGY

### 2.1 *SCaMPR*

The SCaMPR framework was described in Kuligowski (2002). In this framework, brightness temperature values at three GOES infrared channels (6.9, 10.7 and 12.0 or 13.3 μm) are used as predictors of rain rates. In the original implementation, the predictands are rain rate estimates retrieved from passive microwave (PMW) measurements by the Defense Meteorological Satellite Program (DMSP) Special Sensor Microwave/Imager (SSM/I; Ferraro 1997), and by the NOAA Advanced Microwave Sounding Unit-B (AMSU-B; Vila et al. 2007). The PMW rainfall estimates are first used to select the predictors and calibrate the threshold values used to identify rainy and dry pixels. Then in the rainy pixels thus identified, the rain rate predictors are selected from the GOES data and the retrieval equation is calibrated via stepwise forward regression. This calibration is done in real-time as soon as SSM/I and AMSU-B data become available.

The SCaMPR framework has been enhanced to allow the use of precipitation estimates from TRMM Precipitation Radar (TPR; Iguchi et al. 2000) and Microwave Imager (TMI; Kummerow et al. 2001) data as additional predictands. The process starts by aggregating the TMI and TPR data to the resolution of the other PMW data for

*Corresponding author address: Yu Zhang, W/OHD, 1325 East West Highway, Silver Spring, MD 20910; email: yu.zhang@noaa.gov

consistency and then bias-adjusting the SSM/I and AMSU data using TMI data via a distribution-matching procedure similar to that of Joyce et al. (2004). Then the GOES data are aggregated to the resolution of the target data and the results are subsequently used to calibrate the GOES IR-rain rate relation. A schematic of the updated framework is shown in Figure 1.

### 2.2 *Experimental Setup*

We chose central Texas as the location for the evaluation (Fig. 2). Two hundred and forty two rain gauges operated by the Lower Colorado River Authority (LCRA) supply high quality precipitation measurements. The rain gauge data for the period of 2000-7 were acquired from LCRA. Two sets of hourly SCaMPR QPEs were produced at NESDIS for the same period. The first QPE data set was created based on only SSM/I and AMSU data as predictands, which is referred to hereafter as SCaMPR-P (P for passive microwave). The second one was created with the enhanced SCaMPR framework with TPR and TMI data as additional calibration data sets. This data set is referred to as ScaMPR-T (T for TRMM; note that passive microwave data are also used in creating SCaMPR-T).

All of the LCRA gauge records were at an hourly resolution prior to 2005. After 2005, most of the data have been at 15-min scale. These 15-min data were aggregated to hourly. Two steps were undertaken in order to ensure the quality of the gauge records. First, the accumulation by each gauge was plotted over time and any conspicuous discontinuity (i.e., negative increment or positive increment exceeding 300 mm between two consecutive hours) was removed. Then the automated quality assurance (QA) procedure developed by Kondragunta et al. (2006) was applied: records at a particular gauge location were checked against those from neighboring gauges and radar precipitation estimates at the collocated radar bins. The radar-only precipitation estimates used here were created via the Multi-sensor Precipitation Estimator (MPE; see e.g., Young et al., 2000), by using NWS's West Gulf River Forecast Center (WGRFC) archival digital precipitation array (DPA) data for 2000-7. Note that no gauge-based bias correction or multi-sensor merging was performed in order to ensure its comparability to SCaMPR data.

The QA procedure was applied to the hourly and daily gauge products independently. Through the QA procedure, gauge records deemed suspicious were identified and subsequently dropped. The remaining gauge records were then paired with collocated radar and satellite QPEs.

### 2.3 *Evaluation Methods*

The SCaMPR products were evaluated by comparing the quantiles of SCaMPR rainfall amounts at pixels collocated with gauges versus gauge data at both hourly and daily scales. Then the following metrics were computed by aggregating pairs of hourly observations at multiple gauge locations over 2000-7: a) bias (ratio of SCaMPR (or radar) total to gauge total); b) bias of positive pair (where rainfall exceeding 1 mm $h^{-1}$); c) correlation coefficient; d) probability of detection (POD); e) false alarm ratio (FAR; ratio of instances where satellite data indicate rain while gauge data do not); and f) Hedike Skill Score (HSS). POD, FAR and HSS are defined as follows.

Let $c_1$ denote the number of pairs where both gauge and satellite (or radar) report rain below a given threshold, $c_2$ the number of pairs where satellite or radar report rain above this threshold while gauge does not; $c_3$ the number of pairs where gauge reports rain beyond this threshold whereas satellite (or radar) does not, and $c_4$ where both values in the pair are above this threshold, then
:

$$POD = \frac{c_4}{c_3 + c_4}$$

$$FAR = \frac{c_2}{c_2 + c_4}$$

$$HSS = \frac{2(c_1 c_4 - c_2 c_3)}{(c_1 + c_2)(c_2 + c_4) + (c_3 + c_4)(c_1 + c_3)}$$

Among these metrics, bias and correlation were computed in two ways. The first was by using records where either gauge or satellite precipitation estimates were positive ("positive" is defined here as rain rates above 1 mm $h^{-1}$) and the second was by choosing only records where both estimates are positive. POD, FAR and HSS were computed using three precipitation thresholds (1, 5 and 15 mm $h^{-1}$) to investigate the performance of the SCaMPR products at different rainfall intensities (.—The reason thresholds higher than 15 mm

$h^{-1}$ are not shown is that there are few instances that SCaMPR and gauge both report rainfall above 15 $h^{-1}$ for some seasons). These metrics were also computed for the radar-only products to put the accuracy of SCaMPR QPEs into perspective. The evaluation results are stratified by seasons, i.e., December-January-February (DJF; winter), March-April-May (MAM; spring), June-July-August (JJA; summer), September-October-November (SON; fall).

In order to account for the uncertainties associated with the validation statistics, the combined gauge-radar-satellite precipitation estimates were randomly sampled via bootstrapping (Simon, 1997). For each season, 200 samples were drawn from the data set, with each sample half of the size of the entire data set (in terms of number of collated gauge-radar-satellite records). Replicates of records were allowed. The validation statistics were computed for each sample and the associated distribution was derived for each statistic from the multiple samples.

## 3. RESULTS

### 3.1 *Quantile Comparisons*

The quantiles of hourly and daily rainfall are shown in Figs. 3 and 4. On an hourly scale, quantiles from both SCaMPR-P and SCaMPR-T QPE point to a low bias at the higher rain rates, where quantiles from radar-only QPE show much closer agreement to those of the gauge data. Evidently, fewer instances of higher rainfall amounts are present in the SCaMPR-P and SCaMPR-T QPE than in collocated gauge or radar data. Between the two products, quantiles for SCaMPR-T QPE exhibit more severe negative conditional bias for all seasons relative to SCaMPR-P except for spring, where it shows slightly better agreement.

Daily comparisons (Fig. 4) show similar results, except that the low bias in SCaMPR-P and SCaMPR-T products are more pronounced, and especially so for higher daily rainfall amounts (> 50 mm $day^{-1}$). Quantiles from both SCaMPR-P and SCaMPR-T are only slightly different except for DJF, when SCaMPR-P shows closer agreement with the gauge and radar data.

### 3.2 *Comparisons of Hourly Validation Statistics*

Box plots of hourly validation statistics (bias, correlation, POD and FAR) as derived from the sampling exercise are shown in Figure 5. Both SCaMPR-P and SCaMPR-T QPE are positively biased for all four periods (Fig 5a) whereas radar-only data are close to bias-neutral. This positive bias is more pronounced during spring and summer and less so during fall and winter (Fig. 5a). It appears that, though the SCaMPR data exhibit overall positive bias, these data nevertheless are negatively biased at higher rainfall rates in the quantile comparisons. Between these two products, SCaMPR-T is less biased for all four seasons (Fig. 5a). When only records where both gauge and satellite values indicated rain (i.e. > 1 mm $h^{-1}$; such records are hereafter referred to as positive pairs) were included, the bias values for SCaMPR-P and SCaMPR-T QPEs are mixed across seasons. For spring, SCaMPR-P still exhibits conspicuous positive bias, whereas for the other seasons the values are close to bias-neutral with a slightly negative bias in the winter (Fig. 5b). On the other hand, SCaMPR-T is associated with much higher bias values than SCAMPR-P, and the values are negative for all seasons except spring, where it is close to neutral (Fig. 5b). This implies that the addition of the TRMM data had more impact on the absolute rainfall rates than on rainfall detection.

As shown in Figure 5c, correlation values of SCaMPR-T products are generally higher than those for the SCaMPR-P products for all seasons, indicating improvements from incorporating TRMM data. However, even with the improvements, correlation values for SCaMPR-T remain much lower than those for radar QPE (0.2-0.4 for the former vs. 0.6-0.8 for the latter). Correlation values computed using positive pairs (Fig. 5d) point to similar features, except that the improvements of SCaMPR-T over SCaMPR-P are less obvious and are subject to a higher level of uncertainty (as indicated by the wider quantile ranges in Fig. 5d).

The comparisons of probability of detection (POD) and false alarm ratio (FAR) are shown in Figure 5e and 5f. Across the seasons, POD values for SCaMPR-T are consistently lower than those for SCaMPR-P, and the values for these products are much lower than those for the radar QPE. POD values for SCaMPR-P and SCaMPR-T QPEs are

quite low during winter (in the 0.3-0.4 range), and are substantially higher during spring and summer (>0.5). While TRMM ingest tends to reduce POD values, it appears to help mitigate false alarm. For all seasons, FAR values for SCaMPR-T are lower than those for SCaMPR-P.

### 3.3 *Dependence on rainfall intensity*

POD and FAR were also computed by using higher rain rate thresholds (5 mm and 15 mm), and the results are shown in Figures 6 and 7. HSS values are shown in Figure 8.

For POD, it appears that the values for both SCaMPR-P and ScaMPR-T tend to decline with increasing rain rate thresholds irrespective of season (Fig. 6). The difference between the products, i.e., lower POD values for SCaMPR-T, is more pronounced at 5mm except for the winter (Fig. 6). At 15 mm threshold, POD values of both products approach zero (Fig. 6). Compared to the two satellite QPEs, radar-only QPE shows much higher POD across the thresholds and seasons.

FAR values generally increase with higher rainfall thresholds (Fig. 7). SCaMPR-T FAR values are generally superior to SCaMPR-P results. However, at 15 mm $h^{-1}$, SCaMPR-T results show slightly higher FAR values for spring, winter and fall. It needs to be noted that the uncertainties associated with the FAR values are also elevated at 15 mm due to smaller sample sizes. FAR values for ScaMPR-T are far higher than those for radar-only QPE.

HSS values show improvements in SCaMPR-T vs. SCaMPR-P results at 1- and 5-mm thresholds. At the 15-mm threshold, higher HSS values are evident for SCaMPR-P (except for winter, where the HSS score for SCaMPR-T drops to zero due to a lack of data points). Again, HSS values for radar-only QPE are far higher than those for the two satellite products.

## 4. SUMMARY AND PRELIMINARY CONCLUSIONS

Records from 242 rain gauges in central Texas were used to evaluate the accuracy of QPE derived via the original SCaMPR framework and the enhanced one that incorporates TRMM PR and TMI data. Our analyses indicated that ingesting TRMM data helps improve certain aspects of the QPE as judged by the reduction in bias and false alarm rate, and the enhancement in correlation and HSS. However, it tends to introduce negative conditional bias and to suppress the probability of detection. As illustrated in the quantile comparisons, SCaMPR-T products contain fewer higher rainfall values than indicated by SCaMPR-P, and both products show negative biases at higher rain rates in the quantile comparisons despite a presence of positive overall bias in the paired comparison. A closer examination of the SCaMPR QPEs reveals that the instances of false alarms vastly outnumber those in which rainfall was reported by gauges but not by SCaMPR (e.g., by a factor of 2 for SCaMPR-P at 1 mm threshold).

In our analyses, SCaMPR QPEs were shown to exhibit tangible skills in detecting rainfall. Yet, it is also evident that the SCaMPR products are in general much less accurate than the radar-only products. The difference is the most pronounced during heavy rain where the POD values for SCaMPR products, both with and without TRMM ingest, are quite low. Improvement in bias, while evident after the ingest of TRMM, did not translate to improvement in POD. In light of these observations, SCaMPR QPEs can be quite useful in areas without ground radar and gauge coverage. On the other hand, further refinement of the SCaMPR algorithm for improving the detection of heavy rainfall, perhaps by integration of radar observations as an additional predictand, is desirable.

Our evaluation was conducted on hourly and daily scales by using point rain gauge data to determine the effects on TRMM ingest, and perhaps to give guidance to future improvements in the SCaMPR framework. Meanwhile, additional analyses are underway where SCaMPR products are bias-corrected with rain gauge data, and where comparisons of areal averaged rainfall totals and hydrologic simulations will be performed. These analyses will help define the potential use of the SCaMPR products in hydrologic forecasting.

## 5. ACKNOWLEDGEMENTS

We appreciate the assistance of Gregory Shelton and Robert Corby from West Gulf River Forecasts Center in supplying the digital precipitation array data. We are also thankful to Bob Huber at LCRA for providing the rain gauge data, and to Dongsoo Kim at National Climate Data Center (NCDC) for assisting in the acquisition and quality assurance of gauge data.

## 7. REFERENCES


Ferraro, R. R., 1997: Special sensor Microwave Imager derived global rainfall estimates for climatological applications. *J. Geophys. Res*., **102**, 16715-16735

Huffman, G.J., R.F. Adler, D.T. Bolvin, G. Gu, E.J. Nelkin, K.P. Bowman, E.F. Stocker, D.B. Wolff, 2006: The TRMM Multi-satellite Precipitation Analysis: Quasi-Global, Multi-Year, Combined-Sensor Precipitation Estimates at Fine Scale. *J. Hydrometeor.*, **8**, 38–55.

Iguchi, T., T. Kuzo, R. Meneghini, J. Awakw, and K. Okamoto, 2000: Rainprofiling algorithm for the TRMM Precipitation Radar. *J. Appl. Meteor*., **39**, 2038-2052.

Joyce, R.J., J.E. Janowiak, P.A. Arkin, and P. Xie, 2004: CMORPH: A Method that Produces Global Precipitation Estimates from Passive Microwave and Infrared Data at High Spatial and Temporal Resolution. *J. Hydrometeor.*, **5**, 487–503.

Kondragunta, C., D. Kitzmiller, D.-J. Seo, and K Shrestha, 2005: Objective integration of satellite, rain gauge, and radar precipitation estimates in the Multisensor Precipitation Estimator algorithm. *Preprints, 19th Conference on Hydrology,* San Diego, Amer. Meteor. Soc., **2.8**.

Kuligowski, R. J., 2002: A self-calibrating GOES rainfall algorithm for short-term rainfall estimates. *J. Hydrometeor*., **3**, 112-130.

Kummerow, C., Y. Hong, W. S. Olson, S. Yang, R. F. Adler, J. McCollum, R. Ferraro, G. Petty, D. B. Shin, and T. T. Wilheit, 2001: The evolution of the Goddard Profiling Algorithm (GPROF) for rainfall estimation from passive microwave sensors. *J. Appl. Meteor*., **40**, 1801-1820.

Simon J. L. 1997: Resampling: The New Statistics. Available at http://www.resample.com/content/text/index.shtml

Vila, D., R. Ferraro, and R. Joyce, 2007: Evaluation and improvement of AMSU precipitation retrievals. *J. Geophys. Res*., **112**, D20119.

Young, C. B., A. A. Bradley, W. F. Krajewski, A. Kruger, and M. L. Morrissey. 2000. Evaluating NEXRAD multisensor precipitation estimates for operational hydrologic forecasting. *Journal of Hydrometeorology* **1**, 241–254.

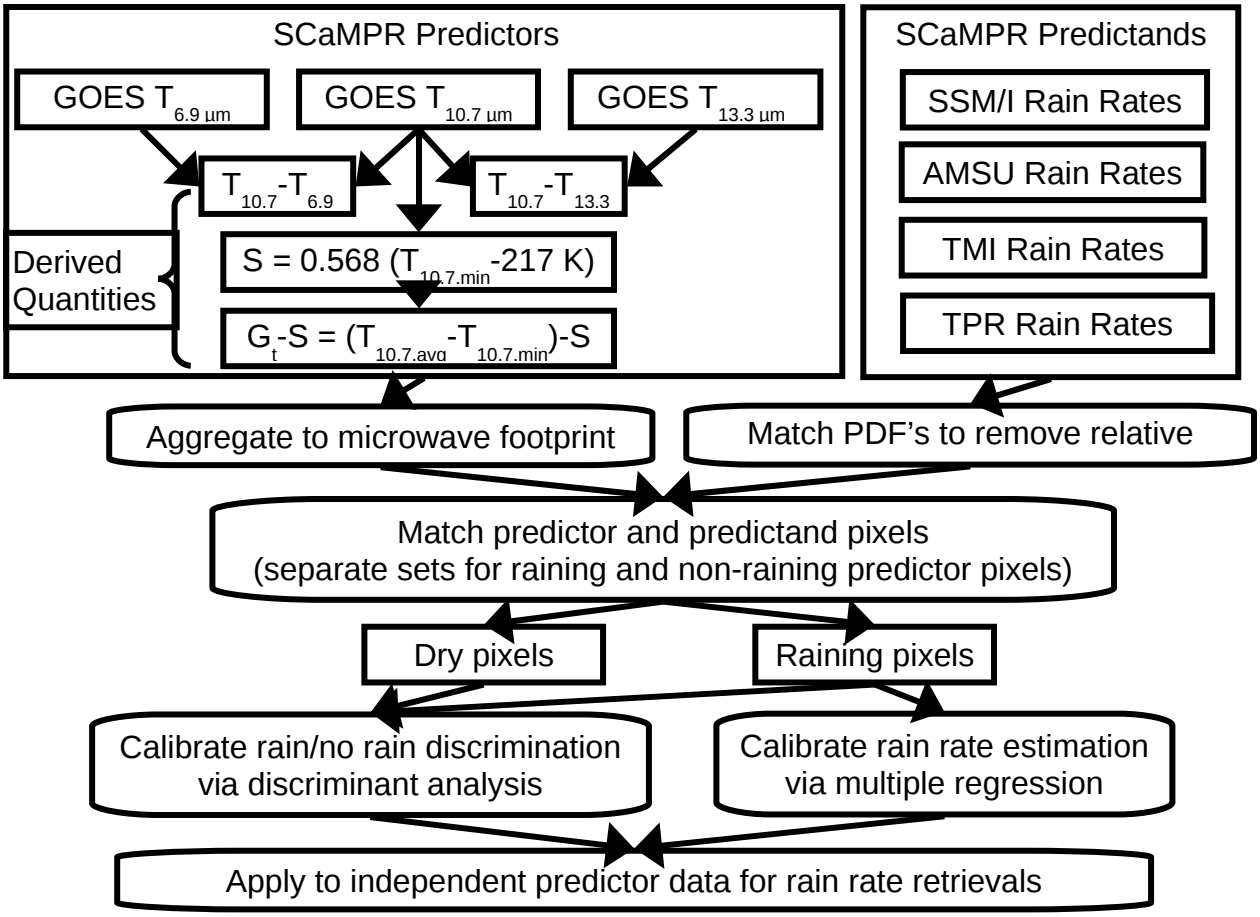


Figure 1: Data flow schematic for the Self-calibrating Multi-satellite Precipitation Retrieval (SCaMPR) algorithm with TRMM ingest.

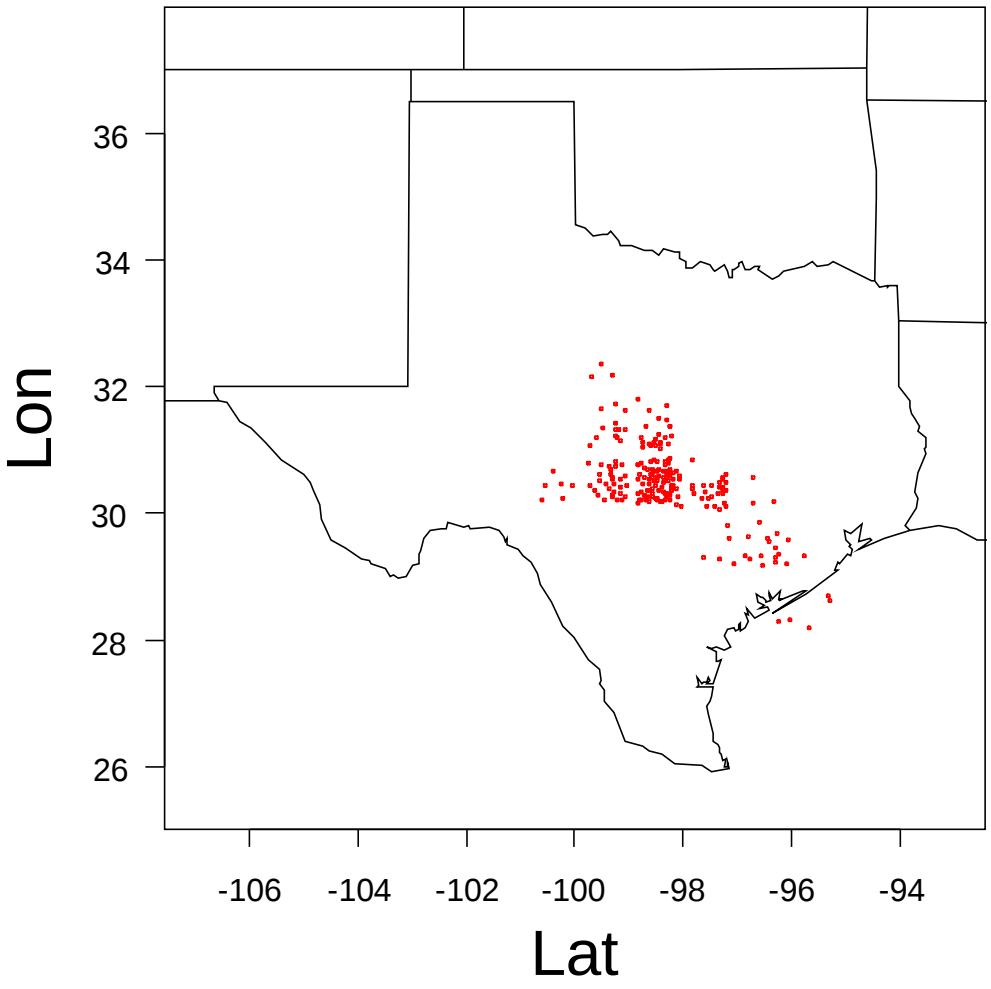


Figure 2: Location of gauges operated by the Lower Colorado River Authority (LCRA).

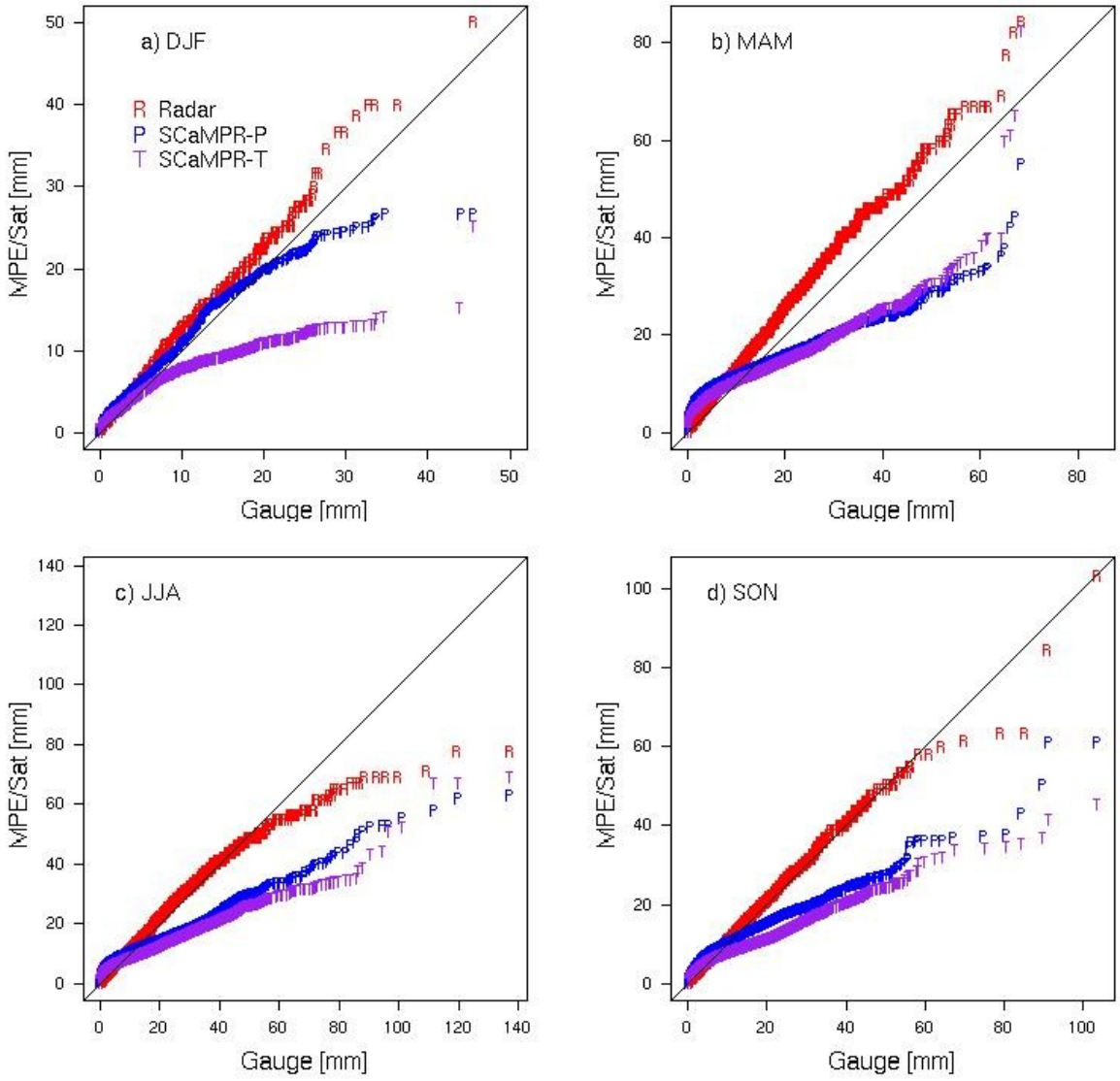


Figure 3: Quantile-quantile plots of hourly rainfall from Radar (R), SCaMPR without TRMM (S), and SCaMPR with TRMM ingest (T), for a) December-January-February, b) March-April-May, c) June-July-August, and d) September-October-November.

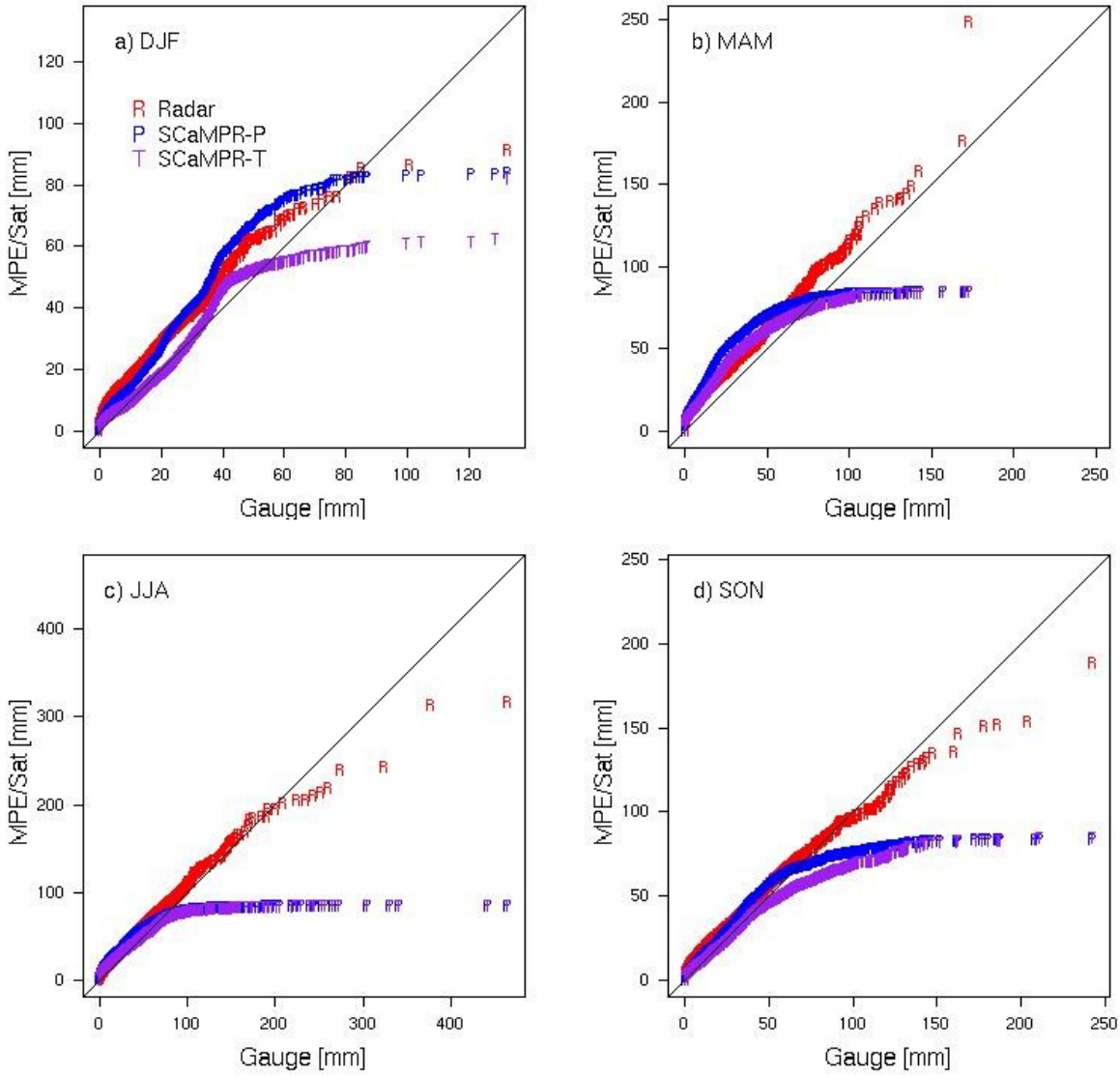


Figure 4: Same as Figure 3 except for daily amounts.

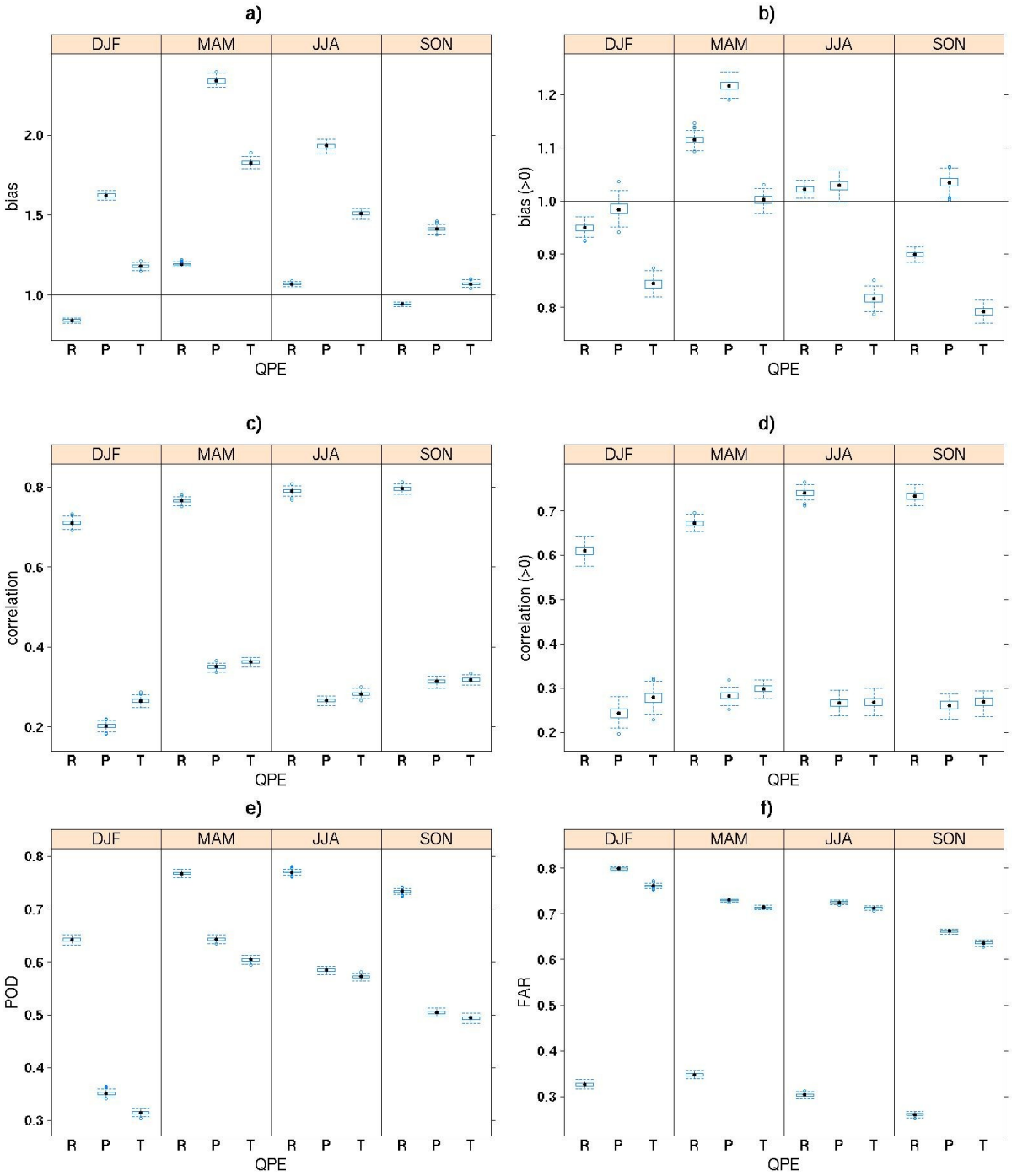


Figure 5: Comparisons of statistics for hourly rainfall from radar and two SCaMPR products: a) bias, b) bias of positive pairs (> 1mm $h^{-1}$), c) linear correlation, d) linear correlation of positive pairs, e) probability of detection, and f) false alarm ratio.

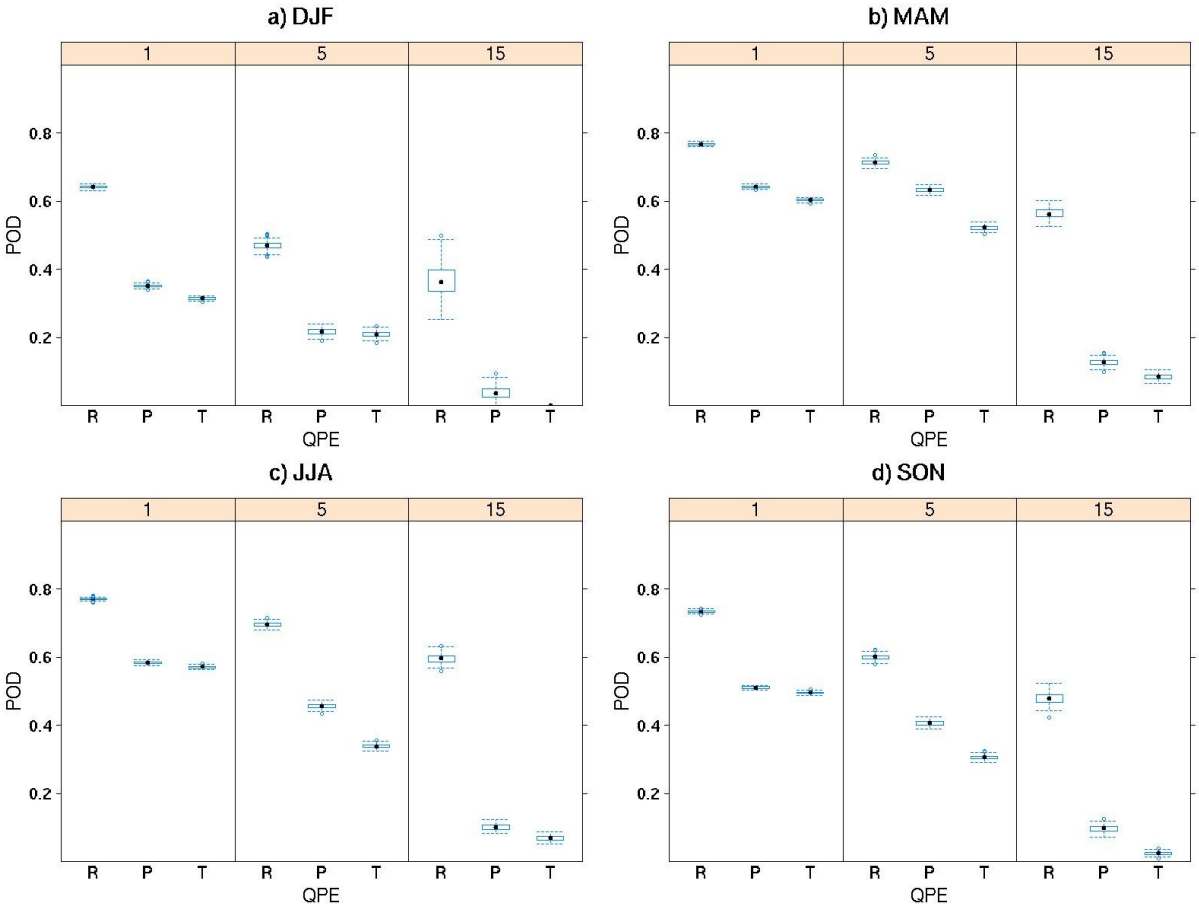


Figure 6: Comparisons of POD for hourly rainfall from radar and two SCaMPR products at 1, 5 and 15 mm thresholds for a) DJF, b) MAM, c) JJA, and d) SON.

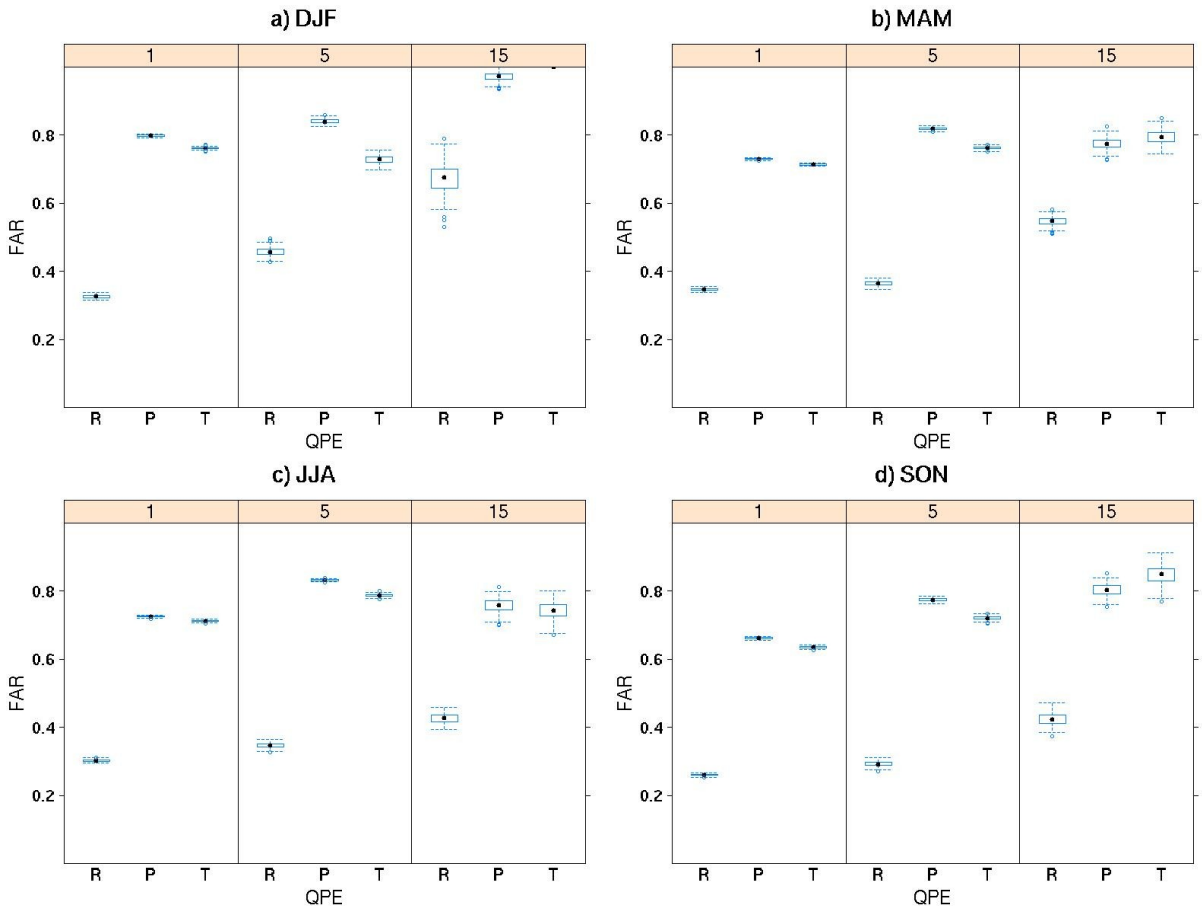


Figure 7: Same as Figure 6, except for FAR.

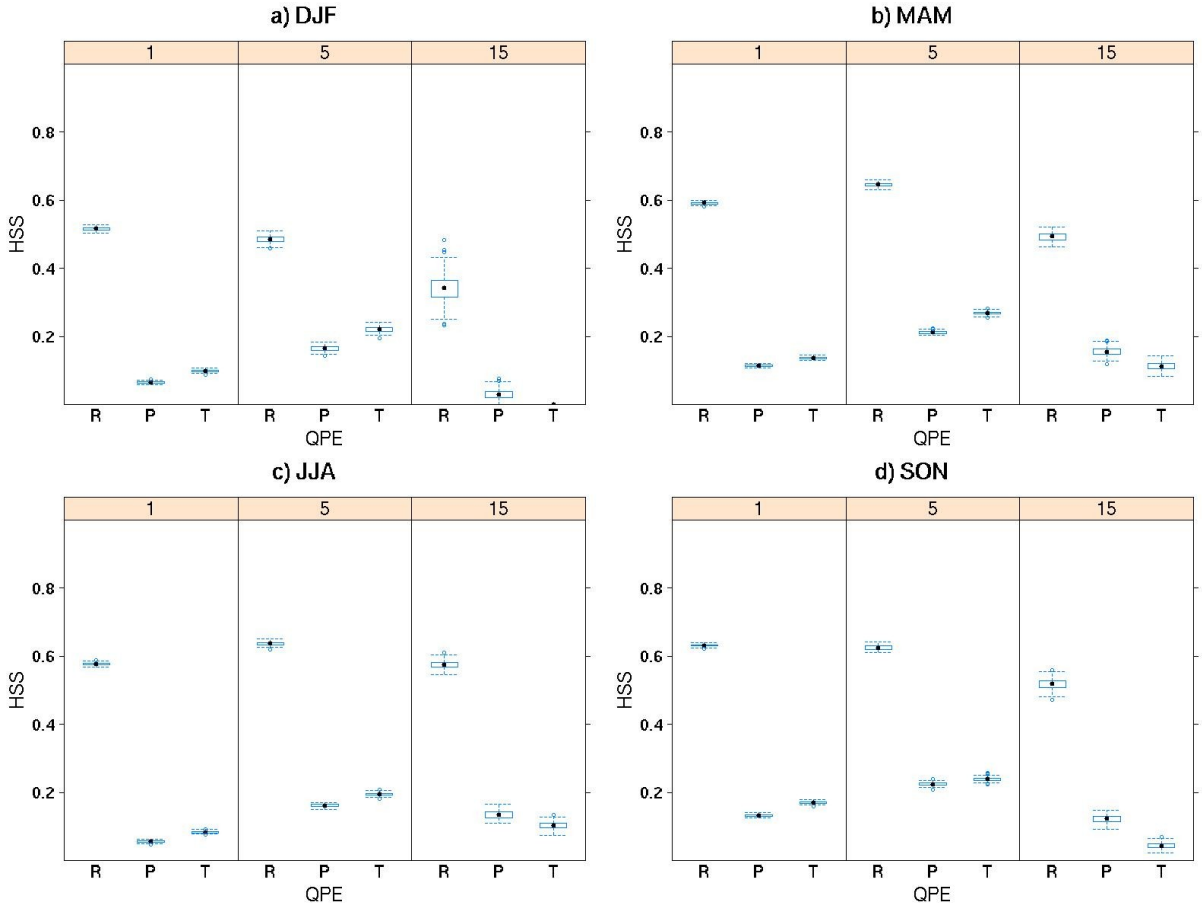


Figure 8: Same as Figure 6, except for HSS.